JOURNAL OF PETROLOGY

Journal of Petrology, 2017, Vol. 58, No. 10, 2035–2053
doi: 10.1093/petrology/egx081
Advance Access Publication Date: 9 January 2018
Original Article

OXFORD

Orientation of Tabular Mafic Intrusions Controls Convective Vigour and Crystallization Style

M. B. Holness[1]*, J. A. Neufeld[1,2,3], A. J. Gilbert[1,2] and R. Macdonald[4,5]

[1]Department of Earth Sciences, University of Cambridge, Downing Street, Cambridge CB2 3EQ, UK; [2]BP Institute for Multiphase Flow, University of Cambridge, Madingley Road, Cambridge CB3 0EZ, UK; [3]Department of Applied Mathematics and Theoretical Physics, University of Cambridge, Centre for Mathematical Sciences, Wilberforce Road, Cambridge CB3 0WA, UK; [4]Institute of Geochemistry, Mineralogy and Petrology, University of Warsaw, 02-089 Warszawa, Poland; [5]Environment Centre, Lancaster University, Lancaster LA1 4YQ, UK

*Corresponding author. Telephone: 01223 333400. Fax: 01223 333450. E-mail: marian@esc.cam.ac.uk

Received October 25, 2016; Accepted December 18, 2017

ABSTRACT

The microstructure in basaltic dykes is significantly different from that in sills and lava lakes of the same bulk composition. For a given width of intrusion (or depth of lava lake), vertical tabular bodies are coarser grained than horizontal bodies, with an invariant plagioclase shape across the intrusion. When comparing samples from sills and dykes for which the average grain size is the same, the dyke samples contain fewer small grains and fewer large grains than the sill samples. In contrast, the variation of median clinopyroxene–plagioclase–plagioclase dihedral angles in dykes correlates precisely with that observed in sills and is a function of the rate of diffusive heat loss. These patterns can be accounted for if the early stages of crystallization in dykes primarily involve the growth of isolated grains suspended in a well-mixed convecting magma, with the final stage (during which dihedral angles form) occurring in a crystal-rich static magma in which heat loss is primarily diffusive. In contrast, crystallization in sills occurs predominantly in marginal solidification fronts, suggesting that any convective motions are insufficient to entrain crystals from the marginal mushy layers and to keep them suspended while they grow. An exception to this general pattern is provided by members of the Mull Solitary Dykes, which propagated 100–1000 km SE from the Mull Palaeogene Igneous Centre, Scotland, through the shallow crust. These dykes, where sampled $>$100 km from Mull, have a microstructure indistinguishable from that of a sill of comparable thickness. We suggest that sufficient nucleation and crystallization occurred in these dykes to increase the viscosity sufficiently to damp convection once unidirectional flow had ceased.

Key words: basalt; crystallization; dyke; plagioclase; sill; convection

INTRODUCTION

The extent and vigour of convection during the solidification of mafic intrusions (sills and larger, more equant, layered intrusions), flows and lava lakes remain controversial (Brandeis & Marsh, 1989; Marsh, 1989, 2015; Worster *et al.*, 1990; Huppert & Turner, 1991; Latypov, 2009). Geological observations used to argue for convection include: evidence for effective magma mixing on a chamber-wide scale, demonstrated by the progressive development of concentric zones containing compositionally identical minerals on the walls, roof and floor of intrusions (e.g. Salmonsen & Tegner, 2013); modal layering attributed to scouring and re-sedimentation of crystals (e.g. McBirney & Nicolas, 1997; Irvine *et al.*, 1998); and the increasing dominance of floor crystallization as the intrusion size increases (Worster *et al.*, 1990), although this has also been used as an argument to support the creation of intrusions by the injection of a succession of crystal-rich slurries (Marsh, 2013). In contrast, the accumulation of crystal cargoes on the floor of sills has been used to argue against convection (Gibb & Henderson, 1992), although a recent re-examination of the olivine distribution on the floor of the Shiant Isles Main Sill found compelling

evidence for settling from a convecting magma (Holness *et al.*, 2016).

It is well understood that liquid cooling at a vertical wall will always be gravitationally unstable. The corollary of this is that, once unidirectional flow through a basaltic dyke has ceased, convection will always occur as long as the viscosity is sufficiently low (e.g. the crystal load is not too high). In comparison, magma in horizontal tabular intrusions will convect only if the critical Rayleigh number is exceeded; this depends not only on viscosity but also on the height of the intrusion, the density change on cooling and/or crystallization, and the thermal gradient in the country rocks. In addition to this fundamental difference between the behaviour of liquids in vertical and horizontal tabular bodies, it is also well known that the microstructure in dykes differs significantly from that in sills: 'The grain size and textures of dikes and sills show marked variations across their widths ... dikes consistently become coarser grained than do sills of comparable thickness formed in the same environment' (Philpotts & Ague, 2009, p. 85).

In this contribution, we examine the microstructures of tabular basaltic intrusions that are thought to have formed from a single injection of magma, focusing in particular on the grain size and shape of plagioclase. We demonstrate that differences in microstructure between sills and dykes are consistent with significant differences in the vigour of convection and style of crystallization as a function of intrusion orientation.

PLAGIOCLASE RECORDS COOLING RATE AND CRYSTALLIZATION TIMESCALE

Plagioclase grain size

The grain size of a rock is the result of the balance between nucleation and growth rates, with coarser grain sizes expected as the cooling rate decreases and crystallization time increases (e.g. Ikeda, 1977; Cashman, 1993). Owing to the high probability of nearby grains impinging on each other, crystals in igneous rocks can grow freely only during the early stages of solidification. Hence, in rocks in which grains are randomly oriented, measures of grain size parallel to the rapid growth direction (i.e. the length of plagioclase tablets) provide information only about solidification prior to significant impingement.

With few exceptions (e.g. Cashman, 1993), since the introduction of the use of the crystal size distribution (CSD) to geological research by Marsh (1988) the CSD of plagioclase, rather than simple measures of average grain size, has been used to constrain the timescales of crystallization of basaltic systems [see Higgins (2006) for a review]. The slope and intercept of CSD plots can be used to constrain either the timescale of crystallization or the growth rate (if the other parameter is known).

Plagioclase grain shape

Experimental work shows that plagioclase grain shape is a function of cooling rate, with thinner laths forming during rapid cooling compared with those grown during slower cooling (Sato, 1995). In dolerite sills and layered intrusions, plagioclase is generally tabular, with the large faces parallel to (010). The three-dimensional (3D) shape of plagioclase cannot be determined straightforwardly from two-dimensional (2D) thin sections of rock containing randomly oriented grains, unless all grains have the same shape. Although this assumption underpins the 2D to 3D conversion method of Higgins (1994), it is unlikely to hold for natural samples (see Mock & Jerram, 2005; Duchêne *et al.*, 2008). However, the average apparent aspect ratio (AR; as viewed in thin section) can be used as a measure of grain shape with no associated assumptions about the 3D shape (Meurer & Boudreau, 1998; Boorman *et al.*, 2004; Holness, 2014). High values of AR are to be expected in samples containing randomly oriented platy grains, whereas low AR is to be expected either in samples containing randomly oriented equant grains, or in samples in which platy grains have a preferred orientation parallel to the plane of the thin section.

Holness (2014) showed that AR for randomly oriented plagioclase varies systematically across dolerite sills and in basaltic lava lakes, with the lowest values (i.e. relatively equant grains) in the slowest-cooled parts of the body (i.e. at, or near, the centre of sills, and in the lower part of lava lakes). Both sills and lava lakes show marginal reversals in AR, perhaps attributable to chilling (Holness, 2014). AR in the central parts of sills of varying thickness is a function of model crystallization time (calculated assuming diffusive heat transport, a country rock temperature of 0°C, and a crystallization interval of 1200–1000°C during which latent heat is released at a constant rate), with a relationship described by

$$\mathrm{AR} = 0{\cdot}5586[6{\cdot}34 - \log(\text{crystallization time in years})].$$

Thus, the highest values of AR (and greater departure from an equant shape) are observed in thin sills, and the lowest values are observed in thick sills (Holness, 2014). Preliminary data from the Skaergaard Layered Series suggest that a similar systematic variation is recorded in the stratigraphy of kilometre-scale layered mafic intrusions (Holness, 2015).

Plagioclase grain shape, as measured by AR, predominantly provides information about the early stages of growth, before the grains impinged against their neighbours. After impingement of randomly oriented grains, further growth is concentrated on the slow-growing (010) faces, leading to a progressive reduction in AR (e.g. Schiavi *et al.*, 2009). The magnitude of this effect has not yet been quantified but, for suites of non-foliated rocks with a broadly similar order of crystallization and liquid line of descent, it is likely to have a uniform effect.

Dihedral angles

Clinopyroxene–plagioclase–plagioclase dihedral angles form during the later stages of solidification.

The geometry of these three-grain junctions in dolerites and gabbros is a function of cooling rate, via the underlying control by the relative growth rates of the different plagioclase crystal faces (Holness, 2015). Median dihedral angles are ~78° in rocks that were fully crystalline within ~1 year, increasing to ~100° for rocks that took ~1000 years to solidify (Holness *et al.*, 2012).

PREVIOUS WORK ON MICROSTRUCTURAL INDICATORS OF MAGMA FLOW AND CONVECTION

Indicators of magmatic flow include attenuation of vesicles (Philpotts & Philpotts, 2007), alignment and imbrication of phenocrysts (Philpotts & Asher, 1994), lineation of crystals (Walker, 1987; Holness & Humphreys, 2003), a preferred orientation of granophyric patches solidified from partial melts derived from the wallrocks (Philpotts & Asher, 1994), and anisotropy of magnetic susceptibility, or AMS (e.g. Knight & Walker, 1988; Tauxe *et al.*, 1998; Abelson *et al.*, 2001; Callot *et al.*, 2001; Féménias *et al.*, 2004; Philpotts & Philpotts, 2007; Magee *et al.*, 2016). Most studies using AMS to detect flow directions through dykes concentrate on the dyke margins to detect the conditions of flow early in the history of dyke emplacement, as the chilled margin is likely to have formed while magma was actively flowing along the conduit (Tauxe *et al.*, 1998; Callot *et al.*, 2001).

Previous work on the microstructural record of convection was based on a consideration of the effect of magma flow on the development of compositional boundary layers around growing crystals and the consequences of this for grain shape. Martin *et al.* (1987) considered the effect of convection via its control on the length-scale of compositional boundary layers. They suggested that growing crystals surrounded by a thin compositional boundary layer are unlikely to have their growth impeded by impingement against crystals nucleating nearby, leading to a habit controlled entirely by the relative rates of growth of the crystal faces. Conversely, if a mushy layer is bathed in a compositional boundary layer thicker than the size of individual crystals it becomes relatively easy to nucleate new crystals close to older crystals, which are thus likely to experience early impingement, leading to a more equant habit [i.e. one affected by impingement rather than one controlled by the relative (unimpeded) growth rates of the different faces].

Kouchi *et al.* (1986) found that stirring during crystallization changes the relationship between crystal morphology and undercooling. In stirred magma at high undercoolings, instead of finding the expected dendritic and spherulitic crystals indicative of diffusion-limited growth (e.g. Lofgren, 1974, 1980), plagioclase and pyroxene are acicular. This is the morphology indicative of crystallization under the interface-controlled growth conditions that occur in static magma at lower undercoolings. The transition from diffusion-limited growth to interface-controlled growth results from the disruption of the compositional boundary layers surrounding the crystals as the experimental charge is stirred.

Higgins (1994) proposed that plagioclase becomes more platy (leading to higher values of AR) if it grows in well-stirred magma. Higgins & Chandrasekharam (2007) developed this concept, citing the results of Kouchi *et al.* (1986) to suggest that (non-dendritic and non-spherulitic) plagioclase departs further from an equant habit (leading to higher AR) as the velocity of liquid flowing past the growing crystal increases. Thus, highly tabular or platy grains are expected to have grown in strongly convecting magmas. However, there are a number of problems with this hypothesis. First, the Kouchi *et al.* (1986) results concern the transition between diffusion-limited and interface-controlled growth and it is not clear that they can be extended to explain variations in shape created entirely during interface-controlled growth. Additionally, the velocity of a crystal relative to the magma in a natural system will be governed by the settling velocity, rather than the convective velocity of the magma (Jambon, 1980), so plagioclase, being almost neutrally buoyant, is unlikely to experience widely varying velocities relative to the magma. Finally, Holness (2014) showed that as sills become thicker (and therefore more likely to convect), plagioclase becomes less platy, in contradiction to the prediction of Higgins & Chandrasekharam (2007).

ANALYTICAL METHODS

Plagioclase grain size

The plagioclase grain size was measured using photomicrographs of the fine-grained samples, whereas images of the coarse-grained samples were obtained with a high-resolution scanner using two polaroid sheets to facilitate distinction between different plagioclase grains. We measured the long-axis lengths of all grains visible in each image. For the very coarsest samples the total number of grains measured was relatively low (with a minimum of 114 grains measured for sample HH-7 from the Hägghult dyke) but generally ~250 grains were measured per sample.

We have chosen to portray the grain-size data in the simplest possible form, with no corrections made to account for measurement in 2D sections. This is because such corrections are dependent on assumptions about grain shape and, while the details of 3D shape are unknown, it is clear from the average apparent aspect ratio that this shape, or range of shapes, changes between samples. We have not calculated CSDs. Instead we portray the data in terms of the average long-axis length, the average area of the grain intersections [calculated as $(\text{average length})^2/\text{AR}$], and the skew of the population of long axes. The grain-size distribution in selected samples is shown in cumulative frequency plots.

Plagioclase grain shape

Average apparent aspect ratios for plagioclase were determined using the same grains for which we measured the long-axis length, following the procedure of Holness (2014). The long and short axes on all grains in any given image were drawn by hand, and the aspect ratio was determined using ImageJ. Between 114 and 392 grains were measured for each sample. The 2σ uncertainties on the average apparent aspect ratio were determined using a bootstrap method based on random sampling of the measurement population.

Dihedral angles

True, 3D, clinopyroxene–plagioclase–plagioclase dihedral angles were measured using a four-axis Leitz universal stage mounted on a James Swift monocular optical microscope, with a UM32 Leitz long working distance objective and a $\times 10$ eyepiece. The median value of a population of angles can be determined satisfactorily with only 25 measurements (Riegger & van Vlack, 1960), although reduction of the 95% confidence intervals about the median to $< \pm 4$–5° [calculated according to the method of Stickels & Hücke (1964)] generally requires more than 50 measurements (Holness, 2010). We report the median values of populations of up to 100 individual measurements of true 3-D dihedral angles in each sample, which were chosen to create a broad range of median angles (i.e. only a few samples were chosen from the margins of the wider dykes, as the field of rapidly cooled samples was adequately populated by samples from the thinner dykes).

GEOLOGICAL EXAMPLES

We used the microstructural information reported by Holness *et al.* (2012) and Holness (2014) for the dihedral angles, plagioclase grain size and grain shape in a series of five basic sills of thickness varying from 3·5 to 366 m. For comparison, we collected microstructural information from a variety of dykes, each of broadly basaltic composition. None of the dykes contains evidence of internal chills indicating a poly-phase intrusion history, and none carried a significant load of phenocrysts.

Three basaltic bodies, part of the Palaeogene Mull Complex, were sampled on the south coast of Mull. The first (Mull dyke 1) is a 3·7 m wide basaltic dyke, sampled at 56·32449°N, 5·93084°E. The second (Mull dyke 2) is 4·6 m wide and was sampled at 56·32466°N, 5·93028°E. The third body is a 14 m wide cone sheet (Mull cone sheet) dipping at ~70° to the north. We sampled this body at 56·31992°N, 5·94362°E, with 10 samples spaced evenly across its width. All three bodies have well-developed chill zones. No geochemical data are available for these three bodies.

We examined samples from two dykes belonging to the Precambrian Blekinge Dalarna Dolerite Group of southern Sweden. These dykes are olivine tholeiites and were emplaced at upper crustal depths into ~1·8 Ga basement (Solyom *et al.*, 1992). The Karlshamn dyke is exposed in a quarry at Stärnö (56·145024°N, 14·848247°E) where it is 151 m wide. A sample traverse was collected along the SW wall of the quarry. The Hägghult dyke is exposed in a quarry west of the town of Lönsboda and samples were collected in a traverse at 56·400559°N, 14·253493°E where the dyke is ~40 m wide.

We examined a Palaeogene basaltic dyke, thought to be related to the nearby Skaergaard Intrusion, collected from NW Kramer Ø, in East Greenland, by T. F. N. Nielsen and C. K. Brooks. This dyke is 10 m wide, with well-developed chilled margins. Bulk compositions of samples from nearby related dykes are provided by Brooks & Nielsen (1978, 1990).

The Moneyacres dyke is one of the Solitary dykes (Geikie, 1897) associated with the Paleogene Mull volcano, forming a swarm extending ~600 km SE of Mull (Macdonald *et al.*, 2010). It is at least 100 km long. Three sample traverses were collected where the dyke crosses the Maich Burn, some 100 km SE of Mull (55·786°N, 4·673°E), two as part of earlier studies (Macdonald *et al.*, 2010) and the third for the present study. The dyke is 13·4 m wide at Maich Burn, with well-developed chilled margins, and the northern side of the dyke is well exposed along the west stream bank, allowing close sample spacing. Exposure of the southern side is fragmentary and relatively inaccessible, with correspondingly fewer samples. The bulk compositions of a selection of Maich Burn samples were reported by Macdonald *et al.* (2010); the rocks are basalts and basaltic andesites and MgO values range from ~7 to 5 wt %. A further traverse was collected some 10 km further to the SE, where the dyke is exposed in a small quarry on East Moneyacres Farm (55·7242°N, 4·5027°E) where the dyke is 32 m wide. One bulk composition from this traverse (for sample EM3) has been provided in the Supplementary Data table of Macdonald *et al.* (2010).

The Lupchinga dolerite dyke belongs to a NNE-trending swarm about 10 km wide and 60 km long, and is exposed on the southern coast of Lupchinga Island in Pääjärvi Lake, Karelia, NW Russia, where it is 22·4 m wide [it was inaccurately described as 21 m wide by Chistyakova & Latypov (2012): R. Latypov, personal communication, 2016]. It has been the focus of a detailed geochemical study by Chistyakova & Latypov (2012), who have provided bulk geochemical analyses of all samples examined as part of the present study. The composition of the dyke is generally uniform (with MgO ~ 5·5 wt %) with a compositionally distinct chilled margin (only one margin is accessible as the other is covered by the sea) with MgO increasing to 5·8 wt %.

The Kestiö dyke is a member of the Åland–Åboland dyke swarm of SW Finland, which forms a NNE-trending zone 40 km wide and 120 km long. Compositionally the dykes are classified as continental tholeiites transitional to alkali basalts (Lindberg *et al.*, 1991; Eklund *et al.*, 1994). The Kestiö dyke occurs on the northwestern shore of Kestiö island, intruding mica

gneisses of the Archean basement. It is 6·75 m wide and was referred to as 'thick dyke' by Chistyakova & Latypov (2009), who undertook a detailed geochemical study of the samples examined here. The dyke has marginal compositional zoning in the chilled outer ~60 cm and a generally compositionally uniform central part.

RESULTS

Plagioclase grain size

Plagioclase grain size, as parameterized by the average apparent long-axis length, is shown as a function of intrusion width in samples from the five sills, eight dykes and the cone sheet (the Moneyacres dyke is sampled in two different places separated by 10 km) in Fig. 1 (data in Table 1). Although average grain size in sills and dykes generally increases with intrusion width, in dykes it increases at a greater rate than it does in sills (Fig. 1), consistent with the observation of Philpotts & Ague (2009). The single exception in our study is the Moneyacres dyke, which is finer grained than expected from comparison with the other dykes: it has a grain size similar to that of sills of the same thickness. The 14 m wide Mull cone sheet is also rather finer grained than might be expected from the other dykes (Fig. 1), but is generally coarser grained than the 13·4 m Moneyacres dyke at Maich Burn.

The average grain size across the Lupchinga dyke, as reported by Chistyakova & Latypov (2012), is significantly different from those reported here. However, their values actually refer to the average length of the 10 largest grains measured (R. Latypov, personal communication, 2016) and, when compared with the average of the 10 largest grains measured as part of this study, there is a close correspondence between their data and ours (Fig. 2).

The average area of grain intersections is shown in Fig. 3, together with the sill data from Holness *et al.* (2012) and Holness (2014), as a function of the theoretical time taken for each sample to crystallize [calculated following Holness *et al.* (2012) assuming diffusive heat loss, a country rock temperature of 0°C, and a crystallization interval of 1200–1000°C during which latent heat is released at a constant rate]. This theoretical time, calculated on the assumption that the sample crystallized in the position it occupies at present, is therefore proportional to the square of the distance from the intrusion margin. We chose to plot average intersection area, instead of average long-axis length, because the trends and patterns are the same in both but the data are more scattered for intersection area, making it easier to distinguish the different dykes.

The average intersection area forms a positive correlation with the calculated crystallization time for the group of sills, which is linear on the log–log plot in Fig. 3—sills become generally coarser grained as their thickness increases and within each sill the grain size increases towards the sill centre. The grain size of the Moneyacres dyke and the other two Mull dykes are indistinguishable from that of the sill samples with the same theoretical crystallization time. The remaining dykes and the cone sheet show a progressively coarser grain size for any given calculated crystallization time, with greater departures from the grain size seen in sill

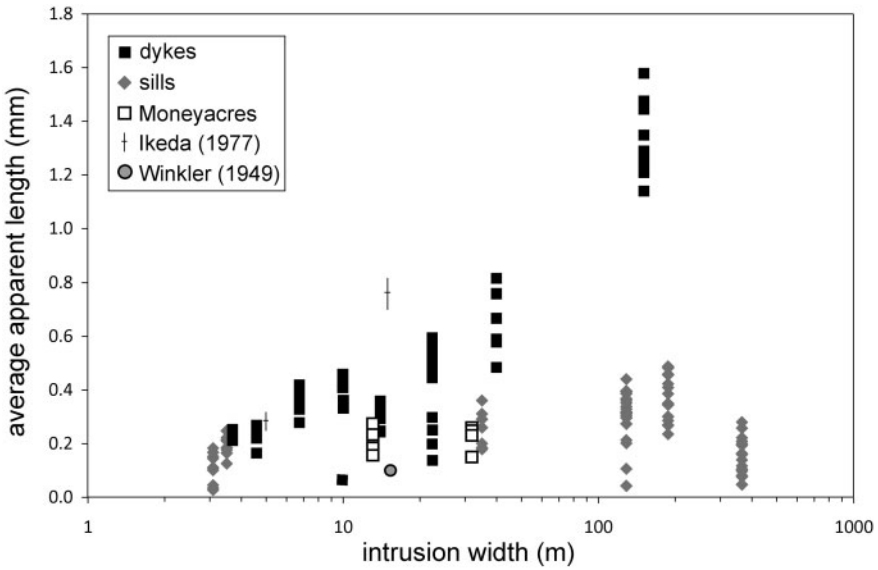

Fig. 1. The average length of plagioclase grains viewed in thin section as a function of width of the host intrusion. Each data point corresponds to a single sample. Whereas the dykes generally show a rapid increase of average grain length with increasing intrusion width, the sills increase in grain size at a slower rate [data from Holness *et al.* (2012)]. The Moneyacres dyke has a grain size similar to that expected for a sill. The average grain sizes are also shown for the 5 m and 15 m Iritono dykes studied by Ikeda (1977) (calculated assuming an average aspect ratio of 3·8–4·2), and the datum for the central part of the Cleveland dyke from Winkler (1949) is also shown. The Ikeda (1977) dykes have a grain size similar to the majority of our dykes, whereas the two Mull Solitary dykes, the Cleveland and the Moneyacres, have similar grain sizes to sills of comparable width.

Table 1: Details of plagioclase grain shape and size, with the median value of the clinopyroxene–plagioclase–plagioclase dihedral angle, Θ_{cpp}

			Plagioclase grain shape				Plagioclase grain size			Dihedral angle	
Sample	Dyke width (m)	Position in dyke (m)	*n*	AR	Min.	Max.	Average	10 largest	Skew	n_a	Θ_{cpp} (deg.)
Mull dyke 1											
M14-20	3·7	3·46	225	4·12	3·92	4·29	0·210	0·432	1·855		
M14-21	3·7	3·14	272	4·10	3·84	4·21	0·222	0·423	0·717	50	77·5 ± 3
M14-22	3·7	2·85	234	4·24	4·02	4·41	0·241	0·563	1·224		
M14-23	3·7	2·25	265	4·20	4·00	4·40	0·236	0·575	2·378	50	82·5 ± 5
M14-24	3·7	1·68	257	4·34	4·12	4·53	0·242	0·557	1·463	60	82 ± 6
M14-25	3·7	1·25	251	4·20	3·94	4·39	0·252	0·573	1·479		
M14-26	3·7	0·45	231	4·24	3·91	4·13	0·225	0·548	1·484	50	78·5 ± 3
M14-27	3·7	0·24	206	4·24	4·12	4·45	0·218	0·553	2·300		
Mull dyke 2											
M14-30	4·6	0·35	113	4·73	4·20	5·20	0·164	0·329	0·913	50	78·5 ± 4
M14-31	4·6	0·90	236	4·15	3·92	4·34	0·219	0·473	0·996	50	78·5 ± 4
M14-32	4·6	2·00	264	4·16	3·92	4·40	0·267	0·588	0·836		
M14-33	4·6	2·70	220	3·99	3·77	4·14	0·237	0·530	1·338	50	79 ± 4
Kestiö dyke											
AL-10/3	6·75	0·4	253	4·19	3·96	4·39	0·277	0·606	0·958		
AL-10/4	6·75	0·8	255	4·14	3·87	4·39	0·353	0·773	0·842		
AL-10/5	6·75	1·05	199	4·16	3·90	4·40	0·417	0·945	0·769		
AL-10/10	6·75	2·75	232	4·11	3·86	4·31	0·327	0·753	0·627		
AL-10/14	6·75	3·7	214	3·92	3·67	4·16	0·412	0·944	0·642	50	80 ± 4
AL-10/18	6·75	5·9	279	3·83	3·59	3·97	0·347	0·798	1·088		
AL-10/19	6·75	6·15	200	4·01	3·79	4·22	0·376	0·850	1·283		
Kramer Ø dyke											
361034	10	1·0	233	3·58	3·37	3·78	0·364	0·886	1·236		
361036	10	3·5	174	3·73	3·53	3·90	0·450	1·006	1·197		
361037	10	6·0	223	3·91	3·65	4·12	0·428	0·957	0·907		
361038	10	8·0	207	3·71	3·51	3·94	0·403	1·065	1·511		
361039	10	9·5	237	3·61	3·39	3·81	0·333	0·745	1·111		
361040	10	9·9	137	3·84	3·65	4·00	0·069	0·124	0·555		
Moneyacres dyke at Maich Burn											
MBA	13·4	0·11		4·50			0·161	0·387	1·301		
MBD	13·4	3·35	349	3·88	3·68	4·08	0·246	0·673	2·330		
MBE	13·4	10·7	233	4·03	3·81	4·26	0·253	0·543	1·300		
MBB	13·4	12·8	229	4·61			0·152	0·378	1·836		
MB1	13·4	0·2	258	4·61	4·38	4·88	0·238	0·704	0·931		
MB2	13·4	0·8	346	4·03	3·75	4·25	0·223	0·527	1·191		
MB3	13·4	2·0	302	3·79	3·55	4·02	0·191	0·439	1·201		
MB4	13·4	3·35	278	3·77	3·52	3·96	0·220	0·535	1·576		
MB5	13·4	4·7	278	3·33	3·16	3·47	0·245	0·575	1·086		
MB6	13·4	5·36	254	3·47	3·27	3·66	0·269	0·703	2·150		
MB7	13·4	6·7	290	3·45	3·27	3·66	0·229	0·549	1·296		
MB10	13·4	1·1	228	4·08	3·87	4·30	0·194	0·451	1·388		
MB11	13·4	2·2	203	3·96	3·64	4·06	0·247	0·566	1·319		
MB12	13·4	3·0	255	3·61	3·44	3·83	0·233	0·531	1·101		
MB13	13·4	4·0	193	3·72	3·50	3·91	0·290	0·750	2·428		
MB14	13·4	5·6	232	3·35	3·15	3·52	0·257	0·611	1·309		
MB15	13·4	7·6	387	3·66	3·45	3·87	0·271	0·687	1·289		
MB16	13·4	9·6	390	3·53	3·41	3·76	0·272	0·632	0·933		
MB17	13·4	12·6	295	4·24	4·01	4·38	0·202	0·455	1·001		
Mull cone sheet											
M14-16	14·0	0·20	124	4·46			0·246	0·521	1·373	50	78 ± 4
M14-18	14·0	0·40	305	3·79	3·57	3·98	0·242	0·575	1·855		
M14-9	14·0	1·20	289	3·87	3·59	4·06	0·307	0·790	1·136	50	79·5 ± 4
M14-10	14·0	2·85	290	4·00	3·74	4·21	0·358	0·908	2·043		
M14-17	14·0	3·60	283	4·06	3·78	4·26	0·316	0·883	1·242		
M14-11	14·0	5·39	344	3·73	3·50	3·97	0·292	0·664	1·120	50	82 ± 3
M14-12	14·0	7·10	276	3·69	3·51	3·89	0·332	0·694	1·091		
M14-14	14·0	11·89	257	4·04	3·78	4·29	0·358	0·783	0·930	50	81 ± 3
M14-15	14·0	13·05	269	3·93	3·70	4·17	0·294	0·675	1·072		
Lupchinga dyke											
mmc1-1/3(3)	22·4	22·08	254	3·67	3·43	3·87	0·198	0·469	1·397		
mmc1-1/1(1)	22·4	21·5	254	3·28	3·07	3·48	0·297	0·638	1·028	50	80·5 ± 3
mmc1-1/23	22·4	20·55	283	3·16	2·99	3·31	0·444	0·996	1·044		
mmc1-1/25	22·4	18·75	228	3·00	2·84	3·18	0·478	1·205	1·136	50	80 ± 4
mmc1-1/27	22·4	16·05	194	3·09	2·90	3·26	0·560	1·244	0·869	40	83 ± 2
mmc1-1/29	22·4	13·95	282	3·21	3·01	3·39	0·550	1·559	1·554		

(continued)

Table 1. Continued

Sample	Dyke width (m)	Position in dyke (m)	Plagioclase grain shape				Plagioclase grain size			Dihedral angle	
			n	AR	Min.	Max.	Average	10 largest	Skew	n_a	Θ_{cpp} (deg.)
Moneyacres dyke at East Moneyacres Farm											
EM1	32·0	2	392	3·65	3·47	3·84	0·149	0·344	1·723		
EM2	32·0	7	303	3·34	3·14	3·48	0·236	0·514	1·315		
EM3	32·0	12	325	3·19	2·97	3·43	0·259	0·619	1·323	50	82·5 ± 3
EM4	32·0	17	288	3·14	2·93	3·30	0·249	0·601	0·963	50	84·5 ± 3
EM5	32·0	22	275	3·14	2·94	3·32	0·247	0·539	0·866	50	82·5 ± 4
EM6	32·0	27	273	3·56	3·24	3·75	0·229	0·563	1·129		
Hägghult dyke											
H-1	40·0	1	220	2·90	2·72	3·07	0·483	1·141	0·797		
H-2	40·0	6	199	3·08	2·88	3·24	0·632	1·512	1·045		
H-3	40·0	12	186	3·32	3·13	3·54	0·755	1·720	1·011		
H-5	40·0	21	151	3·07	2·92	3·19	0·759	2·001	2·285		
H-7	40·0	28	114	3·38	3·22	3·53	0·814	1·756	1·215		
H-8	40·0	36·5	194	2·95	2·75	3·06	0·666	1·611	1·129		
H-9	40·0	38·5	194	3·08	2·9	3·24	0·578	1·197	0·744		
H-10	40·0	39·5	181	3·05	2·86	3·18	0·589	1·213	0·722		
Karlshamn dyke											
KH-1	151·0	1	175	3·21	3·17	3·56	1·139	2·851	1·022		
KH-2	151·0	4	222	3·16	2·96	3·33	1·443	2·876	0·652		
KH-5	151·0	16·9								30	87·5 ± 5
KH-6	151·0	21·8	243	3·20	2·95	3·44	1·242	2·923	1·065	40	88 ± 3
KH-9	151·0	36·4	219	3·19	2·97	3·36	1·278	3·666	2·231		
KH-12	151·0	51	196	3·04	2·84	3·19	1·275	2·895	1·111	30	91·5 ± 4
KH-15	151·0	65·6	181	3·18	2·96	3·35	1·268	3·000	1·607	40	94 ± 2
KH-17	151·0	75·4	158	3·21	3·02	3·37	1·577	3·181	1·055	90	97 ± 2
KH-19	151·0	85·1	199	3·01	2·83	3·17	1·288	2·829	1·166		
KH-22	151·0	99·8	203	3·17	3·00	3·33	1·207	2·967	1·201		
KH-25	151·0	114·4								30	89·5 ± 3
KH-26	151·0	119·3	190	3·02	2·85	3·19	1·348	3·228	1·834		
KH-27	151·0	124·1	195	3·49	3·32	3·67	1·464	2·954	1·009	40	91 ± 2
KH-29	151·0	134·4								30	88 ± 5
KH-30	151·0	139·8	173	3·05	2·89	3·25	1·218	3·204	1·762	30	87·5 ± 2
KH-32	151·0	150·6	182	3·05	2·88	3·18	1·475	3·369	1·029		
KH-33	151·0	150·6								30	85·5 ± 10

The number of grains measured is given by *n*, and the number of three-grain junctions measured is given by n_a. The minimum and maximum values of AR were calculated using a bootstrap method to determine the range of average values from the (unknown) underlying population. The grain size is reported as the average of all long-axis lengths, the average of the 10 longest grains, and the skew of the entire population of grains.

samples with equivalent theoretical thermal histories with increasing dyke width. Most dykes coarsen inwards, in a similar manner to the sills, with the exception of the Karlshamn dyke, which has a constant grain size throughout its 151 m width.

The correlation between intersection area and theoretical cooling time in much of the Lupchinga dyke has a similar slope to that observed in the sills, but in the outermost ~1 m the grain size decreases significantly more rapidly as the margin is approached (Figs 2b and 3). A similar pattern is hinted at in the data from the Kramer Ø dyke, with an apparently anomalously fine-grained sample within a few centimetres of the margin. This marginal break in slope is not apparent in the Mull cone sheet (sampled within 20 cm of the margin), Mull dyke 1 (24 cm from the margin), Mull dyke 2 (35 cm from the margin), or the Moneyacres dyke (12 cm from the margin). The most marginal samples from the Hägghult and Karlshamn dykes were collected ~1 m from the margins and are not significantly fine-grained.

In Fig. 4a, the average length of the 10 largest grains is compared with that of the entire grain population in each sample (data in Table 1). The dykes and sills form distinctly different trends, with the dykes having a smaller difference in length between the 10 largest grains and the entire population. This difference is reflected in the generally smaller (positive) skew of the grain-size population in the dykes (Fig. 4b), consistent with a smaller tail at large grain sizes in any one dyke sample compared with a sill sample with the same average grain size.

The difference in the grain-size population is illustrated in Fig. 5a, in which the cumulative frequency of measured grain lengths is shown for pairs of dyke and

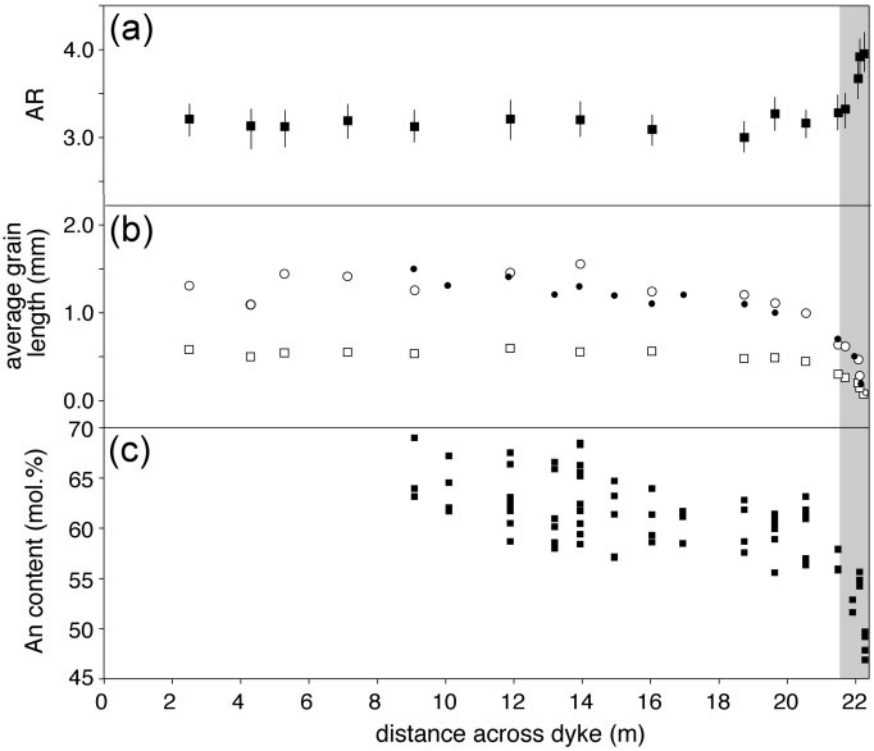

Fig. 2. (a) The average apparent aspect ratio, AR, as a function of position across the Lupchinga dyke. Only one margin is accessible as the other is covered by sea. These data are duplicated in Fig. 7. (b) The average length of plagioclase grains as viewed in thin section in the Lupchinga dyke. Squares show the average length of all grains measured, whereas the open circles show the average length of the 10 largest grains. The dots show the lengths of the 10 largest grains reported by Chistyakova & Latypov (2012). (c) Analyses of plagioclase cores as a function of position in the dyke. Each point represents one grain. Data from Chistyakova & Latypov (2012). The grey box shows the marginal region of the dyke in which AR increases—the five data points in this region form a steep slope on a graph of log grain size vs log crystallization time (Fig. 3).

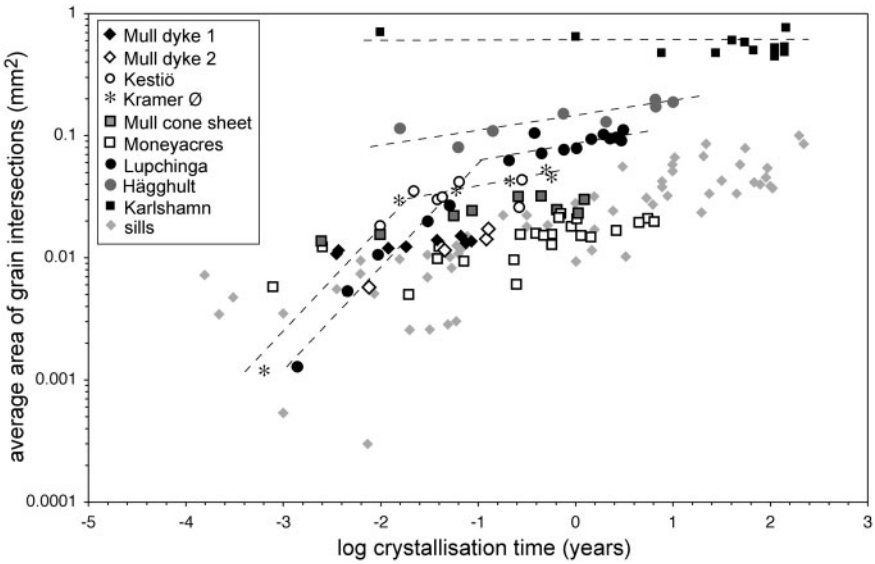

Fig. 3. Average area of plagioclase grain intersections, as viewed in thin section, plotted as a function of a theoretical time for crystallization, calculated assuming each sample crystallized at the position in which it is now found. Calculations are based on the assumptions of a country rock temperature of 0°C, a crystallization interval of 1200–1000°C, a constant release of latent heat and purely diffusive heat loss. The dotted lines are indicative and show a break in slope for the Lupchinga data and a possibly similar break in slope for the Kramer Ø dyke. The invariant grain size across the Karlshamn dyke should be noted.

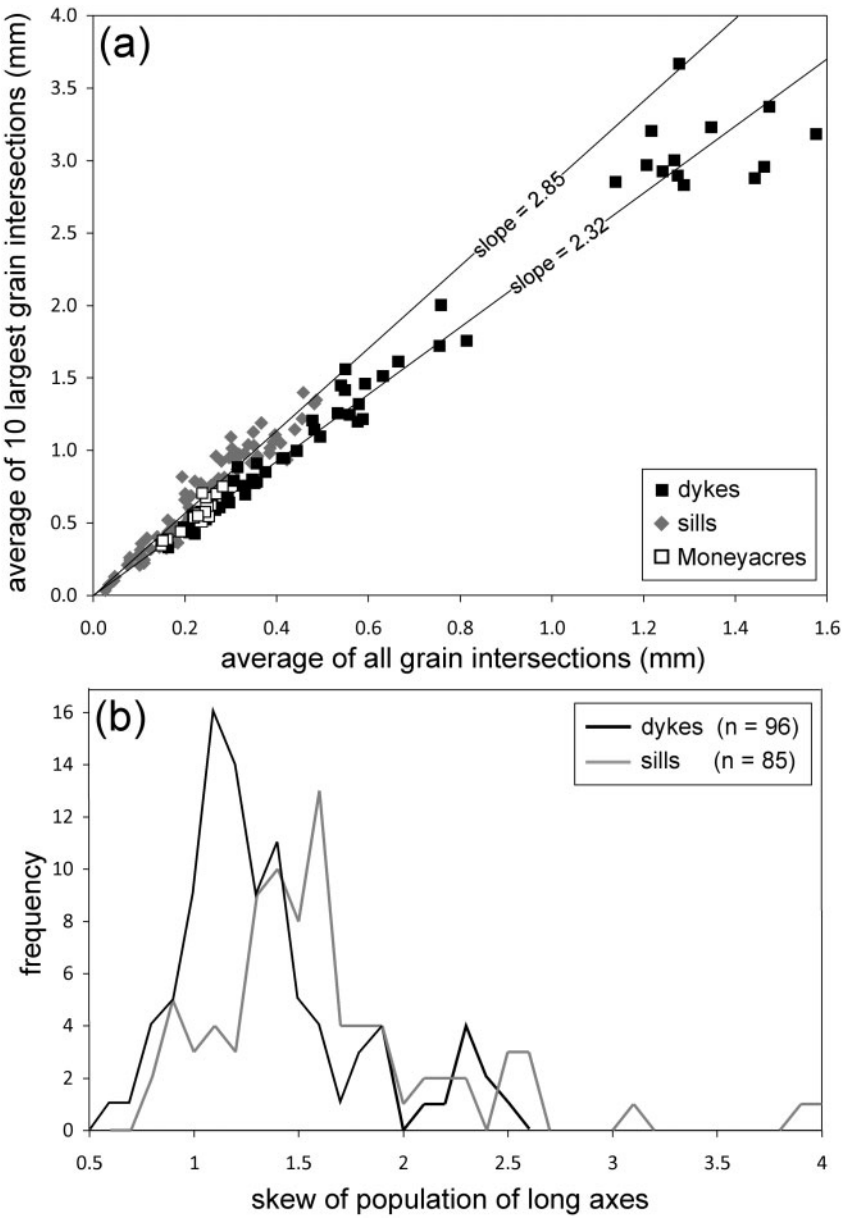

Fig. 4. (a) The average of the 10 longest grains (as viewed in thin section) compared with the average length of the entire grain population. The number of samples in each population is given by *n* in (b). The data for sills and dykes are clearly distinguishable, with different lines of best fit. Sills contain significantly more larger grains than do dykes with the same average grain size. The data from the Moneyacres dyke do not clearly fall into either the dyke or the sill field. (b) A frequency plot of the skews of the grain-size population. In general, the grain-size population in dykes has a smaller positive skew than that in sills. Sills have a significantly longer tail at large grain size than do dykes of a similar average overall grain size.

sill samples with the same average grain length. Dyke samples contain fewer small grains and fewer large grains than the corresponding sill sample. The exception to this is the Moneyacres dyke, for which the grain-size population, as illustrated using cumulative frequencies, is indistinguishable from that of sill samples with the same average plagioclase grain length (Fig. 5b).

Plagioclase grain shape

The range of average apparent aspect ratios in sills and dykes is shown in Fig. 6 as a function of intrusion width. Plagioclase grain shape varies with intrusion width, with lower aspect ratios in the wider intrusions (data in Table 1). Whereas the aspect ratio decreases continuously in sills as the width increases from 3 to 366 m, AR in the 151 m wide Karlshamn dyke is similar to that in the 40 m wide Hägghult dyke, suggestive of a reduction in the sensitivity of grain shape to intrusion width in the widest dykes. In contrast to sills, which commonly show a wide range of AR (correlating with position in the sill), plagioclase grain shape in any dyke is generally less variable: the exception to this is the Moneyacres dyke, which shows as wide a spread as the sills.

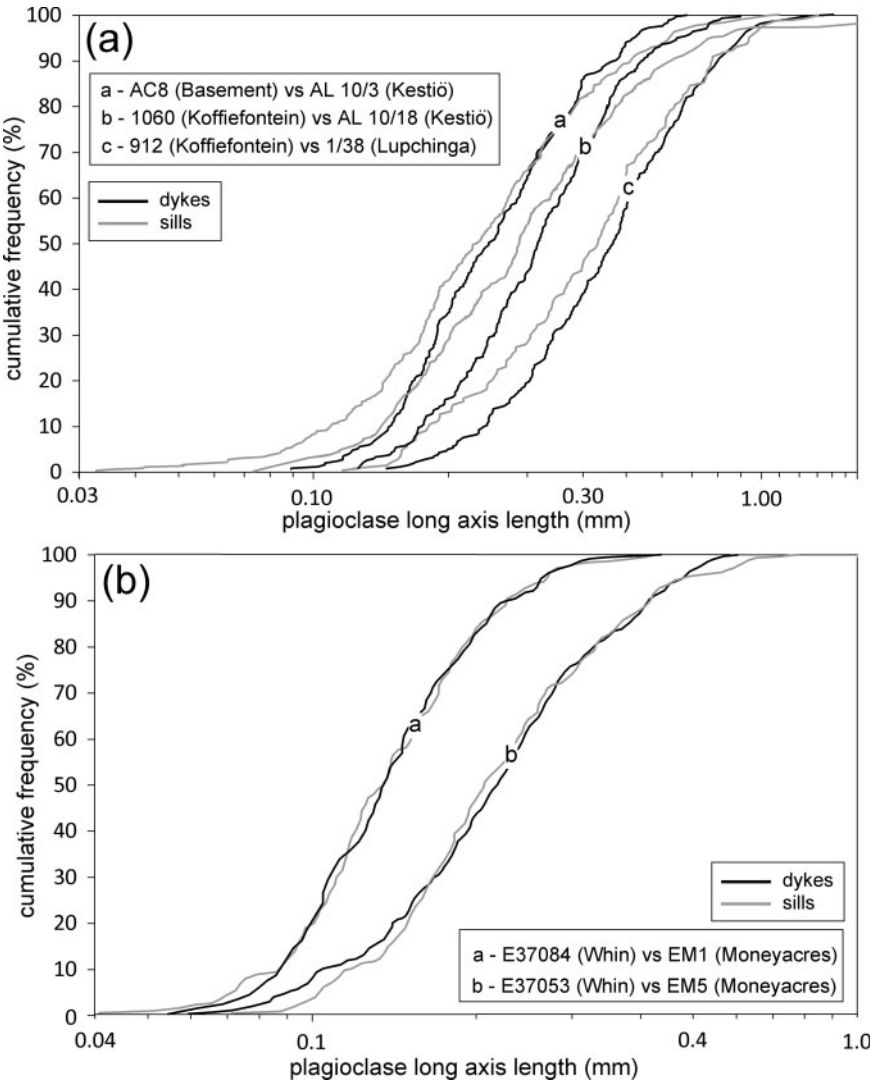

Fig. 5. (a) The cumulative frequency of grain sizes (measured as the length of plagioclase grains as viewed in thin section) in pairs of samples, one from a dyke and one from a sill, each with the same average grain size. It should be noted that for each pair, the sill sample has more smaller grains and more larger grains than the corresponding dyke sample. (b) Pairs of sill and dyke samples, comparing the Moneyacres dyke with samples from the Whin Sill, which have the same average grain size. In contrast to the other dykes, the grain-size distribution in the Moneyacres dyke is indistinguishable from that in sill samples of the same average grain size.

In Fig. 7, AR is shown as a function of position across each of six dykes and the cone sheet (with two traverses across the Moneyacres dyke), in comparison with the values expected from the relationship between average apparent aspect ratio and model crystallization time derived for sills by Holness (2014). The data for the Lupchinga dyke are additionally shown in Fig. 2a. Within error, the plagioclase grain shape is generally invariant across the dykes and cone sheet, with the exception of the Moneyacres dyke, which has AR values that closely approximate the expected values for a sill of the same thickness (Fig. 7). The marginal reversals in AR in sills documented by Holness (2014) are not present either in the cone sheet or in any of the dykes, including the Moneyacres, which are otherwise similar to sills.

Dihedral angles

The median values of the clinopyroxene–plagioclase–plagioclase dihedral angles in the dykes and cone sheet are shown in Fig. 8 (and Table 1), plotted against the calculated model crystallization time. The line through the data in Fig. 8 is the best-fit line through the dataset of dihedral angles collected from the suite of sills (Holness *et al.*, 2012). The dyke data are indistinguishable from dihedral angles in sills of equivalent thickness.

DISCUSSION

Comparisons with earlier work

Direct comparison with earlier work on grain size is not straightforward because there are many different measures of grain size. Ikeda (1977) reported the variation of

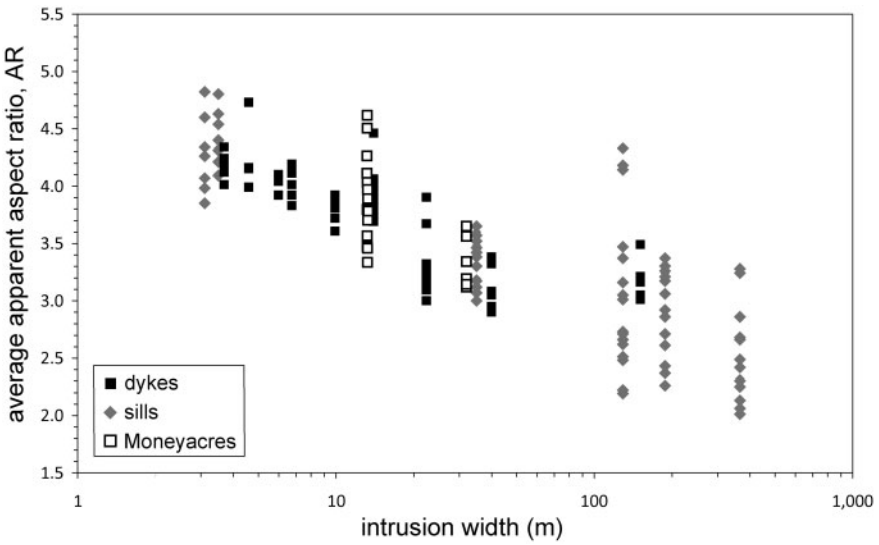

Fig. 6. The average apparent aspect ratio of plagioclase, AR, as a function of intrusion width. The sill data are taken from Holness (2014). Error bars are not included for clarity.

average plagioclase grain size with dyke width, but used the apparent grain width instead of the length as his measure. If we assume that the plagioclase in the two dykes studied by Ikeda (1977) obeys the same relationship between dyke width and average apparent aspect ratio as we observe, then we might expect an AR of ~3·8–4·2 for his two dykes of width 5 and 15 m. His reported average plagioclase widths of 70 μm (for the 5 m dyke) and 190 μm (for the 15 m dyke) would therefore correspond to average lengths of 0·27–0·3 mm and 0·72–0·8 mm (Fig. 1), consistent with our values for dyke grain size.

The Cleveland dyke is another of the Mull Solitaries (Macdonald *et al.*, 1988) and the grain size in this dyke was measured at Great Ayton, Yorkshire by Winkler (1949), some 400 km from the magma source on Mull. The dyke is 16·6 m wide at Great Ayton, and the average grain size of the plagioclase [reported by Winkler (1949) as the average Heywood diameter] for the dyke reaches a maximum of 0·11 mm (Fig. 1). This is significantly finer grained that the 15 m dyke studied by Ikeda (1977), but similar to the grain size we obtain for the Moneyacres dyke and, by comparison with our sill data, for 15 m thick sills.

Convection vs *in situ* crystallization

The larger average grain size and smaller spread of grain sizes in dyke samples compared with sills, and the essentially invariant plagioclase grain shape in dykes, suggest that the early part of the solidification history in tabular intrusions is dependent on intrusion orientation. In contrast, the dihedral angles for sills and dykes are indistinguishable, demonstrating that microstructural development during the later stages of cooling are the same regardless of intrusion orientation. We suggest that this fundamental difference lies in the strength and longevity of convection and the extent to which plagioclase grains grow suspended in a convecting magma or *in situ* on marginal solidification fronts.

Critical to our hypothesis is the assumption that the formation of tabular intrusions involves a first stage during which magma propagates along a planar fracture, and a second stage in which unidirectional flow along the fracture does not occur. Although the first stage may involve considerable flow (e.g. if the dyke or sill is feeding a substantial surface eruption), the second stage probably involves the closing off of the planar intrusion to form an isolated body. If unidirectional flow occurs over relatively short distances in cold crust (e.g. <30 km for upwards flow through the crust), it is likely that most cooling and crystallization occurs once unidirectional flow has ceased. Hence the margins of dykes and sills record only limited crystallization during flow and intrusion filling (and may therefore record some compositional variance compared with the central parts of the intrusion, if the magma changed composition during this initial phase), whereas the central parts record crystallization in a closed magma body. Our hypothesis concerns the behaviour of the magma during this second stage.

If crystallization during the second stage occurs predominantly in inwards-moving solidification fronts on the margins of tabular intrusions (Marsh, 1996), then the shape of the plagioclase will record the crystallization conditions at the position in which it grows and the grain shape will vary systematically through the intrusion: we suggest this is the case for most sills (Fig. 9a). Solidification at any point in the intrusion occurs in the time interval during which the solidification front moves through that position, controlled by the rate of diffusive heat loss through the walls. The grain size at any position will be controlled by the length of this time interval and the nucleation density (which will control the amount of growth on the crystal long axes before

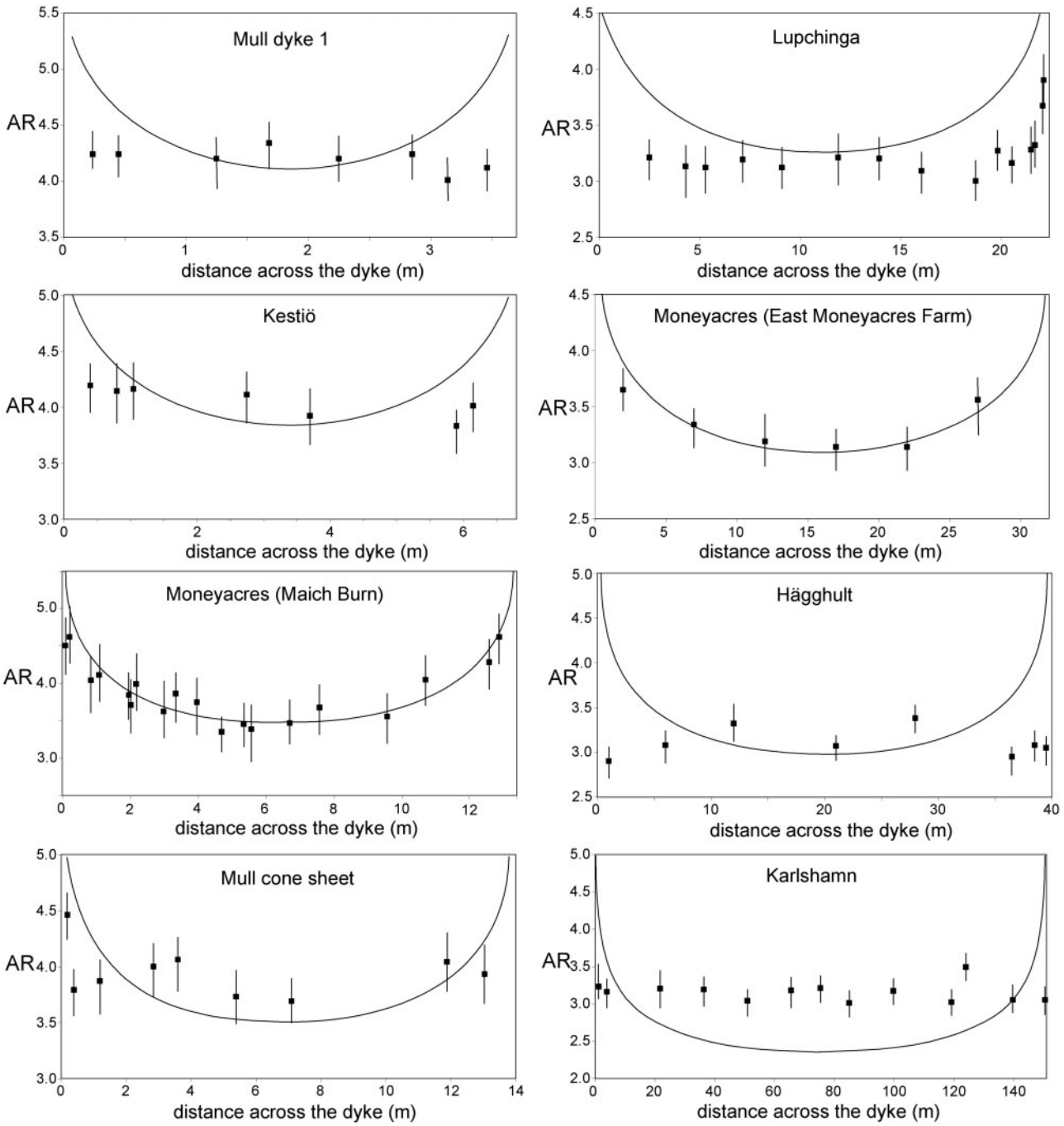

Fig. 7. The average apparent aspect ratio of plagioclase, AR, as a function of position within dykes. In each case the *x*-axis corresponds to the full width of the dyke. The continuous line gives the value of AR expected for a sill, calculated using the expression of Holness (2014).

impingement against neighbouring crystals). During the final stages of solidification, clinopyroxene–plagioclase–plagioclase dihedral angles will form, with values appropriate to the (diffusive) cooling rate experienced at that particular position in the intrusion.

In contrast, if convection is vigorous once unidirectional flow has ceased in the tabular intrusion, crystals nucleated on the intrusion walls during the growth of a chilled margin as the intrusion is filled may be swept into the bulk magma (e.g. secondary nucleation; Melia & Moffitt, 1964) where they will continue to grow as isolated grains or grain clusters suspended in the convecting magma (Fig. 9b). The number of suspended crystals in the convecting interior may be increased if nucleation in the bulk magma is promoted by the addition of supercooled liquid from the wall mushy layer during vigorous convection.

It should be noted that both thermal and compositional gradients, together with variations in the crystal content, may all produce significant density variations

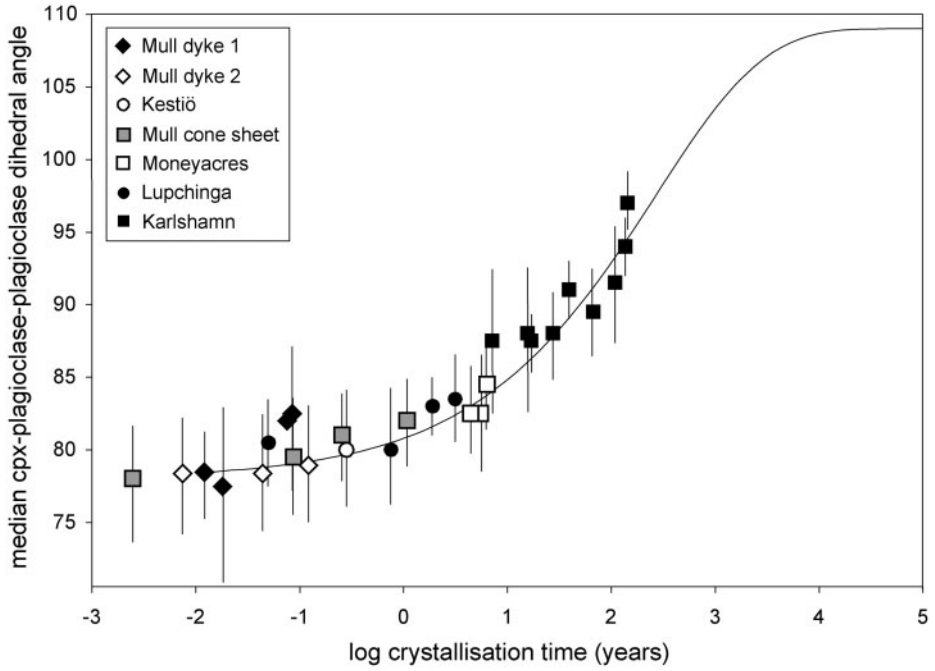

Fig. 8. The median clinopyroxene–plagioclase–plagioclase dihedral angle for dykes, plotted against the model crystallization time calculated assuming diffusive heat loss to a country rock of an initial temperature of 0°C and a crystallization interval of 1200–1000°C. The continuous line gives the line of best fit for sill data from Holness *et al.* (2012) (calculated assuming a minimum value of dihedral angle of 78° and an asymptotic approach to the equilibrium value of 109°).

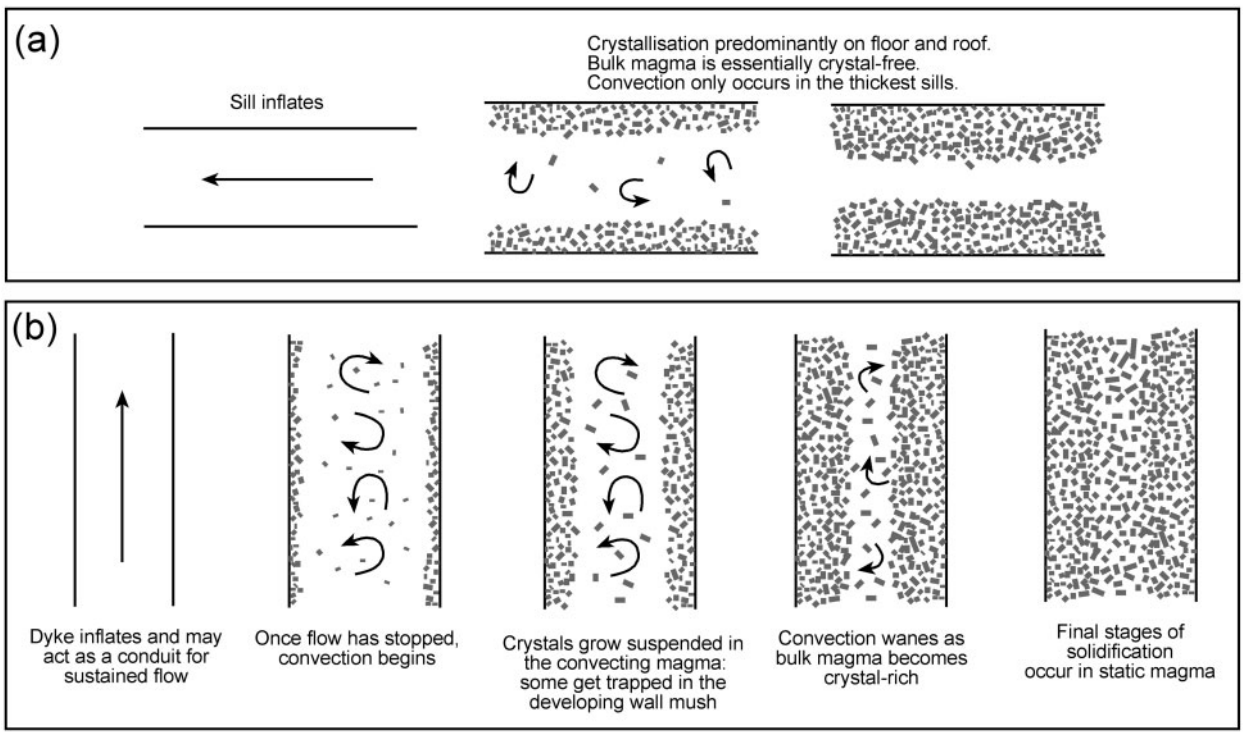

Fig. 9. (a) Crystallization in a horizontal tabular body occurs predominantly in a static, or weakly convecting, magma, with growth of crystals on the floor and roof. (b) Crystallization in a vertical tabular body occurs both at the walls and also in the convecting interior. Suspended crystals have a longer growth time than they would in the corresponding horizontal body, and can grow unimpeded for a significant period. Convection ceases once the magma is sufficiently crystal-rich, with further solidification occurring in a static magma.

that can drive convective flows within the vertical slot. Here, for illustrative purposes, we make a rough estimate of the convective vigour during crystallization of dykes by evaluating the thermal Rayleigh number,

$$Ra = \frac{\rho_0 g \alpha \Delta T L^3}{\kappa \mu}$$

where we take the density $\rho_0 = 2650$ kg m^{-3}, gravity $g = 9{\cdot}81$ m s^{-2}, thermal coefficient of expansion $\alpha = 6{\cdot}45 \times 10^{-5}$ °C^{-1}, thermal diffusivity $\kappa = 8 \times 10^{-7}$ m^2 s^{-1} and viscosity $\mu = 1$–10 Pa s (Martin *et al.*, 1987). Here we use a nominal temperature difference between the dyke interior and the sidewalls, $\Delta T \simeq 10$°C, and, using the width L as the natural length scale, we find characteristically large Rayleigh numbers

$$Ra \simeq 5{\cdot}7 \times 10^7 \text{ to } 1{\cdot}3 \times 10^{15}.$$

These estimates suggest that once unidirectional flow has ceased, convection in basaltic dykes is vigorous, with a nearly uniform interior temperature (Elder, 1965). It may be anticipated that a higher effective Rayleigh number results when the effects of both composition and crystal content are included, but such a condition has not, to our knowledge, been fully explored in the literature.

Nevertheless, for such a rapidly convecting fluid system, the characteristic fluid velocity is (Ng *et al.*, 2015)

$$U_f \simeq \frac{1}{2}(g \alpha \Delta T L)^{1/2}$$

which characterizes a mean thermal wind in the interior of the dyke. In contrast, a simple estimate of the Stokes settling velocity of plagioclase crystals,

$$U_s = \frac{2}{9}\frac{\Delta \rho g L_g^2}{\mu}$$

demonstrates that this is extremely small, with a value of $U_s \simeq 7{\cdot}5 \times 10^{-6}$m s^{-1} for values of the density difference between plagioclase crystals and basaltic melt, $\Delta\rho = 110$ kg m^{-3}, and a crystal size $L_g \simeq 5$mm. The Stokes velocity of plagioclase will therefore generally be sufficiently low compared with typical convective velocities that the crystals do not leave the convecting magma in significant numbers (e.g. Martin & Nokes, 1988, 1989; Lavorel & Le Bars, 2009).

Grains growing suspended in the convecting magma will have a shape governed by the average rate of cooling across the entire convection cell. They will grow as isolated crystals until captured by the wall solidification front (Fig. 9b), and this relatively long period of unimpeded growth will mean they attain a large size. Progressive capture by the inwards propagating wall mush will result in a gradually increasing average grain size towards the centre of the dyke. The differences in grain-size populations (Figs 4 and 5) compared with sills may be accounted for if the very largest grains (with the largest Stokes velocity) leave the convecting magma by flotation or settling, whereas smaller grains may be lost by rapid ripening driven by the temperature fluctuations experienced by grains suspended in a convecting magma (e.g. Mills *et al.*, 2011): these two processes would create a final grain-size population that is narrow in comparison with one of the same average grain size created under static conditions.

In such a model, convection will eventually cease as the load of suspended growing grains increases magma viscosity (Fig. 9b). Once this has happened, further solidification will occur in a static crystal-rich magma, governed by diffusive heat loss. This final stage of solidification will result in overgrowth on the existing grains; the amount of this overgrowth, and the extent to which it may alter the overall plagioclase average aspect ratio, will depend on the amount of liquid remaining when convection ceases. The essentially invariant grain shape across the dykes (which are sampled across a single stratigraphic horizon) suggests only minimal adjustment of the overall grain shape by *in situ* overgrowth. This static phase of solidification also results in clinopyroxene–plagioclase–plagioclase dihedral angles indistinguishable from those developed in a body that cooled entirely by diffusion.

According to this model, solidification in sills occurs primarily in solidification fronts on the sill floor and roof, with the bulk magma being essentially crystal-free. In contrast, the early solidification of dykes is dominated by the growth of isolated crystals suspended in a convecting magma. Convection ceases in dykes once the crystal load is sufficiently high, leading to a final stage of static solidification of relatively crystal-rich homogeneous magma. The precise details of the variation of microstructure across the dyke will depend on the extent to which crystallization occurred on the walls, the extent to which these wall crystals were scoured by the convection, and the rate at which the wall crystal mush propagated relative to the cessation of convection in the interior. These will in turn be controlled by the rate of heat loss to the walls, the original crystal load of the dyke and the presence or absence of exsolving volatile phases.

Do all dykes convect?

The Mull cone sheet, dipping at 70°, has a grain size intermediate between that expected for sills and that expected for fully convecting dykes (Fig. 1). Although this suggests crystallization behaviour intermediate between one involving growth predominantly in marginal solidification fronts and one dominated in the early stages by growth of grains suspended in a convecting magma, the plagioclase grain shape is generally invariant across the width of the sheet (Fig. 7), consistent with crystallization in a convecting magma body. The single data point suggestive of *in situ* growth in a solidification front (close to the left wall, Fig. 7) is intriguing, but we would anticipate that dips much shallower than 70° should be adequate to change the crystallization behaviour from sill-like to dyke-like. Further

work should be aimed at characterizing the microstructure of tabular bodies oriented at various angles to the horizontal to determine the critical orientation that triggers this change in behaviour.

The Moneyacres dyke is an outlier in microstructural terms, containing plagioclase with grain size (Fig. 1), grain-size distribution (Fig. 5a) and shape (Fig. 7) indistinguishable from that of a sill of comparable thickness. According to the model outlined above, the Moneyacres dyke must therefore have crystallized by the inwards migration of solidification fronts. The fine grain size of the Cleveland dyke reported by Winkler (1949) suggests that this dyke also crystallized in the absence of convection strong enough to keep crystals suspended. Both dykes are part of the swarm that propagated up to 1000 km southeastwards through the shallow crust from their source on Mull (Macdonald *et al.*, 1988). It is therefore likely that significant nucleation and crystal growth occurred both during initial dyke propagation and as magma continued to flow in the resultant conduits, with crystallites from the chilled margin entrained into the flowing magma (e.g. Macdonald *et al.*, 1988). Once unidirectional flow had ceased, the magma would therefore contain a large number of crystals and crystallites compared with a magma that had propagated only a short distance through cold crust, and convection would therefore be weak or short-lived.

Although the available compositional evidence for the particular dykes described here suggests that they are predominantly of uniform composition in their central regions, many dykes show significant compositional variation across their width (e.g. Philpotts, 1998). Some of these dykes may be composite, with successive intrusions bringing in magma of different composition into a body that was already sufficiently solid to permit the creation of a distinct later intrusion. However, we suggest that significant compositional variation across the width of dykes that preserve no evidence for internal chill zones may be indicative that convection in such dykes was either weak or very short-lived; this could be tested by an examination of microstructure.

Why is evidence for convection in dykes not evident in AMS studies?

There is an abundant literature describing constraints on magma flow directions in dykes using anisotropy of magnetic susceptibility (AMS). Most of these studies are concentrated on the marginal portions of dykes, to detect the conditions of flow early in the history of dyke emplacement and to ensure that solidification took place while unidirectional flow was still occurring (e.g. Tauxe *et al.*, 1998; Callot *et al.*, 2001; Magee *et al.*, 2016). Many studies are focused on thin dykes (e.g. Knight & Walker, 1988; Philpotts & Philpotts, 2007; Magee *et al.*, 2012) and the fast cooling rates of these bodies mean that it is less likely that convection was a significant process during crystallization. Notably, Knight & Walker (1988) found that a consistent flow direction was not seen in the widest dyke (3·5 m) they examined and suggested that this is a consequence of turbulent flow (e.g. Huppert & Sparks, 1985). However, it is also possible that once dykes become wider than 3·5 m the magma cools sufficiently slowly that it has time for convection to be established once unidirectional flow has ceased: vigorous convection would result in a widely variable fabric preserved in the fully solidified dyke.

Nkono *et al.* (2006) used AMS to examine the variation of flow direction across two wide dykes (5·5 and 23 m) and found evidence for consistent laminar magma flow across both: it appears that neither of these dykes convected once unidirectional flow had ceased. Importantly, both are relatively silica-rich basaltic andesites with a significant load of amphibole and biotite phenocrysts: it is therefore possible that the viscosity was sufficiently high to damp convection in a similar manner to that postulated for the Moneyacres dyke. Future work should be aimed at investigating the links between consistent flow directions across dykes and sills and microstructural parameters such as grain size and shape and the phenocryst load.

Chill zones

Several intriguing questions arise from our observations of microstructures in the margins of tabular intrusions. First, values of AR in the margins of dykes do not show the marginal reversals that are a feature of sills and lava lakes (Holness, 2014), even for the Moneyacres dyke, which otherwise has a microstructure indistinguishable from that of a sill. Second, several dykes have a complex relationship between grain size and position in the dyke, with a stronger positive correlation in the outermost regions compared with the centre. The dyke that shows this best is the Lupchinga, which also shows an associated smoothly outwards increase in AR in the marginal 1 m (Fig. 2a).

The margins of intrusions record the earliest parts of the solidification history, although sustained flow of magma within conduits will melt back any early-formed chills (Bruce & Huppert, 1989, 1990). It is possible that early-formed chills may also be eroded during sustained convection, either by melt-back if the intrusion is sufficiently large, or by plucking of crystals from the developing solidification front. The absence of marginal reversals may be because the earliest stage of solidification is not preserved in dykes, and we are therefore sampling some later stage once the solidification front was able to develop.

A further complication may arise if the width of the dyke changes during filling or conduit flow, or once flow has ceased. The width of dykes is controlled by a complex series of factors including the magmastatic pressure in the source magma chamber and the regional stress field. Although it is accepted that magma-filled fractures can widen on the addition of

further magma, such fractures may also become narrower if the pressure in the magma is insufficient to overcome the regional compressive stress field. The microstructure in the dyke margins may therefore have formed while the dyke was at a different width from that finally preserved.

The Lupchinga chill has been very extensively analysed by Chistyakova & Latypov (2012), who found significant compositional variation in the outermost parts. The anorthite content of the plagioclase decreases rapidly in the outermost 1 m, with a weakly developed trend towards more primitive compositions in the dyke centre (Fig. 2c), attesting to the filling of the dyke by magma of varying composition. These compositional variations have been used to argue that the Lupchinga dyke records solidification during continuous flow of magma of progressively changing composition (Chistyakova & Latypov, 2012). Prolonged magma flow in the dyke would result in the loss of well-developed chill zones (e.g. Bruce & Huppert, 1989, 1990) and the development of a wide contact aureole (e.g. Holness & Humphreys, 2003). The associated heating of the country rocks would result in Θ_{cpp} being higher than that in equivalent sill samples. Although we have no information about the contact aureole of the Lupchinga dyke, it has a well-developed chill zone and dihedral angles indistinguishable from values observed in sills (Fig. 8). We therefore suggest that the Lupchinga dyke developed in two distinct stages, the first involving the creation of a narrow dyke filled with relatively evolved liquid, which solidified from the margins with no significant convection, creating a smooth trend of inwards decreasing AR in a fine-grained matrix. Before the first batch was fully solidified the dyke was inflated by the arrival of a second batch of magma—this batch convected, resulting in uniform AR and a relatively coarse grain size. The weakly developed increase in anorthite content towards the centre of the dyke (i.e. not including the chill zone, shaded in Fig. 2c) could be a consequence of small batches of magma being added to the dyke during late-stage inflation.

Accordingly, the filling history of each dyke is critical in determining its microstructural development, with a slow incremental filling creating a well-defined chill zone with sill-like features and possibly also a distinct composition. The microstructure at the margins will also depend on whether the dyke represents a long-lived conduit or single injection. The final important factor is the load of crystallites in the magma once flow has stopped. The first two factors control the microstructure of the edges (Is there a chill? How thick is the chill?) whereas the third controls whether or not convection can occur.

What is still not clear is why horizontal tabular bodies exhibit marginal reversals in AR, instead of the steadily increasing values that might be expected for the shorter crystallization interval at the margin (and that are observed in the Moneyacres dyke and, in the model outlined above, in the Lupchinga dyke). Holness (2014) suggested that the reversals may be a consequence of abundant nucleation and early impingement in chilled margins, but if this were so we might expect to see reversal in dykes.

The relationship between dihedral angle and grain shape

A critical difference between sills and dykes is that, in the former, dihedral angle variation maps onto variation of plagioclase aspect ratio, whereas in the latter these two parameters are decoupled. Holness (2015) showed that the underlying control on dihedral angle is the response of growth rates of different crystal faces of plagioclase to changes in cooling rates. The decoupling between these two parameters in the dykes can be explained if the growth patterns of plagioclase change once it is trapped in the solidification front—once convection has stopped, plagioclase grows according to its position in the dyke and therefore the final stages of solidification, during which dihedral angles are formed, record the local cooling regime, rather than an averaged regime. That the second growth stage does not significantly change the overall grain shape of the plagioclase suggests that it is the first growth stage that is the dominant control on the final shape. Grain shape therefore largely records the pre-impingement growth of crystals, which occurs at the solidification front early in the evolution of the magmatic intrusion, whereas dihedral angle is largely controlled by the diffusive cooling of the late-stage, stagnant intrusion and country rock as the remaining vestiges of residual melt are cooled and crystallized.

CONCLUSIONS

Building on the initial observation of Philpotts & Ague (2009), we have demonstrated that there commonly are significant microstructural differences between basaltic dykes and sills. For a given width of intrusion, vertical (or steeply dipping) tabular bodies are coarser grained, with an invariant plagioclase shape across the intrusion. When comparing samples from sills and dykes for which the average grain size is the same, the dyke samples contain fewer small grains and fewer large grains than the sill sample. In contrast, the variation of median clinopyroxene–plagioclase–plagioclase dihedral angles in dykes correlates precisely with that observed in sills and is a function of rate of diffusive heat loss. These patterns can be accounted for if the early stages of crystallization in dykes occur primarily by the growth of isolated grains suspended in a convecting magma, with the final stage (during which dihedral angles form) occurring in a crystal-rich static magma in which heat loss is primarily diffusive. In contrast, crystallization in sills of thickness up to 366 m occurs predominantly in marginal solidification fronts, suggesting that any convective motions in the sills that we examined are insufficient to entrain crystals from the marginal mushy layers

and to keep them suspended while they grow. The spatial variation of AR in lava lakes (Holness, 2014) suggests that these, too, behave like sills. Importantly, the microstructural distinctions we have detected between dykes and sills (and lava lakes) can be used only to detect vigorous convection: it is entirely possible that convection occurred in the sills, but it was not sufficiently strong to disrupt the solidification fronts and to prevent them being the primary locus of crystal growth.

The Moneyacres (and probably also the Cleveland) dyke is an exception to this pattern, with microstructural features indistinguishable from that of a sill of comparable thickness. It is probable that some nucleation and crystallization occurred in these two dykes during the extended propagation through the (cold) shallow crust from their source >100 km from the sampling sites.

Further work should be aimed at collecting AMS data for dykes and cone sheets with a variety of orientations to detect whether or not there is a consistent magnetic fabric across their width. Such data should be compared with plagioclase grain shape and size to test the hypothesis that these microstructural characteristics can be used as an indicator for convection. Dykes with distinct compositional zonation across their width should also be examined to detect whether they have microstructures consistent with an essentially crystal-free, weakly (or non-) convecting magma.

ACKNOWLEDGEMENTS

We are grateful to Ulf Söderlund and Leif Johansson, who collected the samples of the Karlshamn and Hägghult dykes; to Rais Latypov, who loaned samples of the Kestiö and Lupchinga dykes; to Troels Nielsen, who sent us samples of the Kramer Ø dyke; and to Bill Budenberg and Stephen Siklos, who helped collect samples on Mull. John MacGillivray and Dugie MacInnes very helpfully reaffirmed the locations of the two traverses across the Moneyacres Dyke and we are grateful to them for the confirmation of GPS coordinates. We acknowledge supportive and insightful reviews from George Bergantz, Rais Latypov, Craig Magee and Bruce Marsh.

FUNDING

A.J.G. acknowledges an NERC CASE studentship award (grant number D07591442: MA-2013-00657). J.A.N. is supported by a Royal Society University Research Fellowship. This work was supported by the Natural Environment Research Council (grant numbers NE/J021520/1 and NE/N009894/1).

REFERENCES

Abelson, M., Baer, G. & Agnon, A. (2001). Evidence from gabbro of the Troodos ophiolite for lateral magma transport along a slow-spreading mid-ocean ridge. *Nature* **409**, 72–75.

Boorman, S., Boudreau, A. & Kruger, F. J. (2004). The Lower Zone–Critical Zone transition of the Bushveld Complex: a quantitative textural study. *Journal of Petrology* **45**, 1209–1235.

Brandeis, G. & Marsh, B. D. (1989). The convective liquidus in a solidifying magma chamber: a fluid dynamic investigation. *Nature* **339**, 613–616.

Brooks, C. K. & Nielsen, T. F. D. (1978). Early stages in the differentiation of the Skaergaard magma as revealed by a closely related suite of dike rocks. *Lithos* **11**, 1–14.

Brooks, C. K. & Nielsen, T. F. D. (1990). A discussion of Hunter and Sparks (Contrib Mineral Petrol 95: 451–461). *Contributions to Mineralogy and Petrology* **104**, 244–247.

Bruce, P. M. & Huppert, H. E. (1989). Thermal control of basaltic fissure eruptions. *Nature* **342**, 665–667.

Bruce, P. M. & Huppert, H. E. (1990). Solidification and melting along dykes by the laminar flow of basaltic magma. In: Ryan, M. P. (ed.) *Magma Transport and Storage*. Chichester: John Wiley, pp. 87–101.

Callot, J.-P., Geoffroy, L., Auborg, C., Pozzi, J. P. & Mege, D. (2001). Magma flow directions of shallow dykes from the East Greenland volcanic margin inferred from magnetic fabric studies. *Tectonophysics* **335**, 313–329.

Cashman, K. V. (1993). Relationship between plagioclase crystallization and cooling rate in basaltic melts. *Contributions to Mineralogy and Petrology* **113**, 126–142.

Chistyakova, S. Y. & Latypov, R. (2009). Two independent processes responsible for compositional zonation in mafic dykes of the Åland–Åboland dyke swarm, Kestiö Island, SW Finland. *Lithos* **112**, 382–396.

Chistyakova, S. & Latypov, R. (2012). Magma differentiation and crystallization in basaltic conduits by two competing petrogenetic processes. *Lithos* **148**, 142–161.

Duchêne, S., Pupier, E., Le Carlier de Veslud, C. & Toplis, M. J. (2008). A 3D reconstruction of plagioclase crystals in a synthetic basalt. *American Mineralogist* **93**, 893–901.

Eklund, O., Fröjdö, S. & Lindberg, B. (1994). Magma mixing, the petrogenetic link between anorthositic suites and rapakivi granites, Åland. SW Finland. *Mineralogy and Petrology* **50**, 3–19.

Elder, J. W. (1965). Turbulent free convection in a vertical slot. *Journal of Fluid Mechanics* **23**, 99–111.

Féménias, O., Diot, H., Berza, T., Gauffriau, A. & Demaiffe, D. (2004). Asymmetrical to symmetrical magnetic fabrics of dikes: paleo-flow orientations and paleo-stresses recorded on feeder-bodies from the Motru Dike Swarm (Romania). *Journal of Structural Geology* **26**, 1401–1418.

Geikie, A. (1897). *Ancient Volcanoes of Great Britain, Vol. II*. London: Macmillan.

Gibb, F. G. F. & Henderson, C. M. B. (1992). Convection and crystal settling in sills. *Contributions to Mineralogy and Petrology* **109**, 538–545.

Higgins, M. D. (1994). Numerical modeling of crystal shapes in thin sections: estimation of crystal habit and true size. *American Mineralogist* **79**, 113–119.

Higgins, M. D. (2006). *Quantitative Textural Measurements in Igneous and Metamorphic Petrology*. Cambridge: Cambridge University Press.

Higgins, M. D. & Chandrasekharam, D. (2007). Nature of sub-volcanic magma chambers, Deccan Province, India: evidence from quantitative textural analysis of plagioclase megacrysts in the Giant Plagioclase Basalts. *Journal of Petrology* **48**, 885–900.

Holness, M. B. (2010). Decoding dihedral angles in melt-bearing and solidified rocks. *Journal of the Virtual Explorer* **35**, paper 3, doi:10.3809/jvirtex.2010.00265.

Holness, M. B. (2014). The effect of crystallization time on plagioclase grain shape. *Contributions to Mineralogy and Petrology* **168**, 1076.

Holness, M. B. (2015). Plagioclase growth rates control three-grain junction geometry in dolerites and gabbros. *Journal of Petrology* **56**, 2117–2144.

Holness, M. B. & Humphreys, M. C. S. (2003). The Traigh Bhàn na Sgùrra sill, Isle of Mull: flow localization in a major magma conduit. *Journal of Petrology* **44**, 1961–1976.

Holness, M. B., Richardson, C. & Helz, R. T. (2012). Disequilibrium dihedral angles in dolerite sills: a new proxy for cooling rate. *Geology* **40**, 795–798.

Holness, M. B., Farr, R. & Neufeld, J. A. (2016). Crystal settling and convection in the Shiant Isles Main Sill. *Contributions to Mineralogy and Petrology* **172**, article 7, doi:10.1007/s00410-016-1325-x.

Huppert, H. E. & Sparks, R. S. J. (1985). Cooling and contamination of mafic and ultramafic magmas during ascent through continental crust. *Earth and Planetary Science Letters* **74**, 371–386.

Huppert, H. E. & Turner, J. S. (1991). Comments on 'On convective style and vigor in sheet-like magma chambers' by Bruce D. Marsh. *Journal of Petrology* **32**, 851–854.

Ikeda, Y. (1977). Grain size of plagioclase of the basaltic andesite dikes, Iritono, central Abukuma plateau. *Canadian Journal of Earth Science* **14**, 1860–1866.

Irvine, T. N., Andersen, J. C. Ø. & Brooks, C. K. (1998). Included blocks (and blocks within blocks) in the Skaergaard intrusion: geological relations and the origins of rhythmic modally graded layers. *Geological Society of America Bulletin* **110**, 1398–1447.

Jambon, A. (1980). Diffusion cationique dans les silicates fondus: étude expérimentale et modèles pétrologiques. PhD thesis, University of Orleans.

Knight, M. D. & Walker, G. P. L. (1988). Magma flow directions in dikes of the Koolau Complex, Oahu, determined from magnetic fabric studies. *Journal of Geophysical Research* **93**, 4301–4319.

Kouchi, A., Tsuchiyama, A. & Sunagawa, I. (1986). Effect of stirring on crystallisation kinetics of basalt: texture and element partitioning. *Contributions to Mineralogy and Petrology* **93**, 429–438.

Latypov, R. (2009). Testing the validity of the petrological hypothesis 'no phenocrysts, no post-emplacement differentiation'. *Journal of Petrology* **50**, 1047–1069.

Lavorel, G. & Le Bars, M. (2009). Sedimentation of particles in a vigorously convecting fluid. *Physical Review E* **80**, 046324.

Lindberg, B., Eklund, O. & Suominen, V. (1991). Middle Proterozoic, Subjotnian diabases and related mafic rocks in the archipelago of southwestern Finland. In: Laitakari, I. (ed.) *IGCP-257 Fennoscandian Meeting and Excursion on Precambrian Dyke Swarms. IGCP-257 Technical Report* **4**, 18–30.

Lofgren, G. E. (1974). An experimental study of plagioclase crystal morphology: isothermal crystallization. *American Journal of Science* **274**, 243–273.

Lofgren, G. E. (1980). Experimental studies on the dynamic crystallization of silicate melts. In: Hargraves, R. B. (ed.) *Physics of Magmatic Processes*. Princeton, NJ: Princeton University Press, pp. 487–551.

Macdonald, R., Wilson, L., Thorpe, R. S. & Martin, A. (1988). Emplacement of the Cleveland dyke: evidence from geochemistry, mineralogy and physical modelling. *Journal of Petrology* **29**, 559–583.

Macdonald, R., Bagínski, B., Upton, B. G. J., Pinkerton, H., MacInnes, D. A. & MacGillivray, J. C. (2010). The Mull Palaeogene dyke swarm: insights into the evolution of the Mull igneous centre and dyke emplacement mechanisms. *Mineralogical Magazine* **74**, 601–622.

Magee, C., Stevenson, C., O'Driscoll, B., Schofield, N. & McDermott, K. (2012). An alternative emplacement model for the classic Ardnamurchan cone sheet swarm, NW Scotland, involving lateral magma supply via regional dykes. *Journal of Structural Geology* **43**, 73–91.

Magee, C., O'Driscoll, B., Petronis, M. S. & Stevenson C. T. E. (2016). Three-dimensional magma flow dynamics within subvolcanic sheet intrusions. *Geosphere* **12**, 842–866.

Marsh, B. D. (1988). Crystal size distribution (CSD) in rocks and the kinetics and dynamics of crystallization I. *Theory. Contributions to Mineralogy and Petrology* **99**, 277–291.

Marsh, B. D. (1989). On convective style and vigor in sheet-like magma chambers. *Journal of Petrology* **30**, 479–530.

Marsh, B. D. (1996). Solidification fronts and magmatic evolution. *Mineralogical Magazine* **60**, 5–40.

Marsh, B. D. (2013). On some fundamentals of igneous petrology. *Contributions to Mineralogy and Petrology* **166**, 665–690.

Marsh, B. D. (2015). Reply. *Contributions to Mineralogy and Petrology* **169**, 21, doi:10.1007/s00410-015-1110-2.

Martin, D. & Nokes, R. (1988). Crystal settling in a vigorously convecting magma chamber. *Nature* **332**, 534–536.

Martin, D. & Nokes, R. (1989). A fluid-dynamical study of crystal settling in convecting magmas. *Journal of Petrology* **30**, 1471–1500.

Martin, D., Griffiths, R. W. & Campbell, I. H. (1987). Compositional and thermal convection in magma chambers. *Contributions to Mineralogy and Petrology* **96**, 465–475.

McBirney, A. R. & Nicolas, A. (1997). The Skaergaard Layered Series. Part II. Magmatic flow and dynamic layering. *Journal of Petrology* **38**, 569–580.

Melia, T. P. & Moffitt, W. P. (1964). Crystallisation from aqueous solution. *Journal of Colloid Science* **19**, 433–447.

Meurer, W. P. & Boudreau, A. E. (1998). Compaction of igneous cumulates, Part II: Compaction and the development of igneous foliations. *Journal of Geology* **106**, 293–304.

Mills, R. D., Ratner, J. J. & Glazner, A. F. (2011). Experimental evidence for crystal coarsening and fabric development during temperature cycling. *Geology* **39**, 1139–1142.

Mock, A. & Jerram, D. A. (2005). Crystal size distributions (CSD) in three dimensions: insights from the 3D reconstruction of a highly porphyritic rhyolite. *Journal of Petrology* **46**, 1525–1541.

Ng, C. S., Ooi, A., Lohse, D. & Chung, D. (2015). Vertical natural convection: application of the unifying theory of thermal convection. *Journal of Fluid Mechanics* **764**, 349–361.

Nkono, C., Féménias, O., Diot, H., Berza, T. & Demaiffe, D. (2006). Flowage differentiation in an andesitic dyke of the Motru Dyke Swarm (Southern Carpathians, Romania) inferred from AMS, CSD and geochemistry. *Journal of Volcanology and Geothermal Research* **154**, 201–221.

Philpotts, A. R. (1998). Nature of a flood-basalt-magma reservoir based on the compositional variation in a single flood-basalt flow and its feeder dike in the Mesozoic Hartford Basin, Connecticut. *Contributions to Mineralogy and Petrology* **133**, 69–82.

Philpotts, A. R. & Ague, J. (2009). *Principles of Igneous and Metamorphic Petrology*. Cambridge: Cambridge University Press.

Philpotts, A. R. & Asher, P. M. (1994). Magmatic flow-direction indicators in a giant diabase feeder dike, Connecticut. *Geology* **22**, 363–366.

Philpotts, A. R. & Philpotts, D. E. (2007). Upward and downward flow in a camptonite dike as recorded by deformed vesicles and the anisotropy of magnetic susceptibility (AMS). *Journal of Volcanology and Geothermal Research* **161**, 81–94.

Riegger, O. K. & van Vlack, L. H. (1960). Dihedral angle measurements. *Transactions of the Metallurgical Society of the AIME* **218**, 933–935.

Salmonsen, L. P. & Tegner, C. (2013). Crystallisation sequence of the Upper Border Series of the Skaergaard Intrusion: revised subdivision and implications for chamber-scale magma homogeneity. *Contributions to Mineralogy and Petrology* **165**, 1155–1171.

Sato, H. (1995). Textural difference between pahoehoe and aa lavas of Izu-Oshima volcano, Japan—an experimental study on population density of plagioclase. *Journal of Volcanology and Geothermal Research* **66**, 101–113.

Schiavi, F., Walte, N. & Keppler, H. (2009). First *in situ* observation of crystallization processes in a basaltic–andesitic melt with the moissanite cell. *Geology* **37**, 963–966.

Solyom, Z., Lindqvist, J.-E. & Johansson, I. (1992). The geochemistry, genesis, and geotectonic setting of Proterozoic mafic dyke swarms in southern and central Sweden. *GFF* **114**, 47–65.

Stickels, C. A. & Hücke, E. E. (1964). Measurement of dihedral angles. *Transactions of the Metallurgical Society of the AIME* **230**, 795–801.

Tauxe, L., Gee, J. S. & Staudigel, H. (1998). Flow directions in dikes from anisotropy of magnetic susceptibility data: the bootstrap way. *Journal of Geophysical Research* **103**, 17775–17790.

Walker, G. P. L. (1987). The dike complex of Koolau volcano, Oahu: internal structure of a Hawaiian rift zone. In: Decker, R. W., Wright, T. L. & Stauffer, P. H. (eds) *Volcanism in Hawaii, 2. US Geological Survey, Professional Papers* **1350**, 961–993.

Winkler, H. G. F. (1949). Crystallisation of basaltic magma as recorded by variation in crystal size in dikes. *Mineralogical Magazine* **28**, 557–574.

Worster, M. G., Huppert, H. E. & Sparks, R. S. J. (1990). Convection and crystallization in magma cooled from above. *Earth and Planetary Science Letters* **101**, 78–89.